Chapter 2

Dynamic light scattering studies on a lyotropic discotic nematic liquid crystal

2.1 Introduction

Lyotropic liquid crystal phases are mostly exhibited by surfactant molecules dissolved in a polar solvent like water. Generally, surfactant molecules are amphiphilic having a hydrophobic part and a polar hydrophilic part [1]. Above a certain concentration, these molecules aggregate and form micelles or layered structures. These systems are important because they find many useful applications in our daily life. One material that exhibits lyotropic liquid crystalline behavior is the simple household soap. Other diverse applications also exist for amphiphilic molecules because they can dissolve both polar and nonpolar substances. Lyotropic liquid crystals can be used to make stable hydrocarbon foams. Lyotropic liquid crystals are also important because of their role in biology. The outer most layer of skin is primarily a lyotropic liquid crystal made of fatty acids.

Cesium perfluoro-octanoate (CSPFO), a salt of short chain perfluorocarboxylic acid, is a surfactant. These molecules when dissolved in water form disk-like micelles over a range of concentration. CSPFO-water system exhibits a lamellar phase, a discotic nematic (N_D) phase and an isotropic phase on heating [2]. A schematic diagram of various phases shown by CSPFO water system is depicted in Fig. 2.1. In this system, the N_D phase is found to be stable over a wide range of concentration and temperature. CSPFO in water is a well studied system. A high resolution phase diagram of this system has been reported [3].

In this chapter, we describe our studies on N_D phase of CSPFO water system. We employ dynamic light scattering (DLS) to measure the twist viscoelastic coefficient of this system. DLS is a very useful technique to investigate the dynamics of a given medium [4]. In liquid crystals, DLS studies yield relaxation times of the viscoelastic modes arising due to thermal fluctuations. There are many reports on the DLS studies of viscoelastic response of thermotropic liquid crystals [5–10]. However, relatively less attention has been paid on lyotropic systems, despite their wide applications in biology and related fields. Duke and Du Pre [11] have studied lyotropic cholesteric liquid crystals. Lacerda Santos *et. al.* [12, 13] have carried out Rayleigh scattering on nematics of cylindrical micelles and disk-like micelles to compare the diffusivities. Recently, Yamamoto and Tanaka have studied an inverse micellar system consisting of a ternary mixture of a thermotropic liquid crystal, surfactant and water [14].

(a)   (b)   (c)
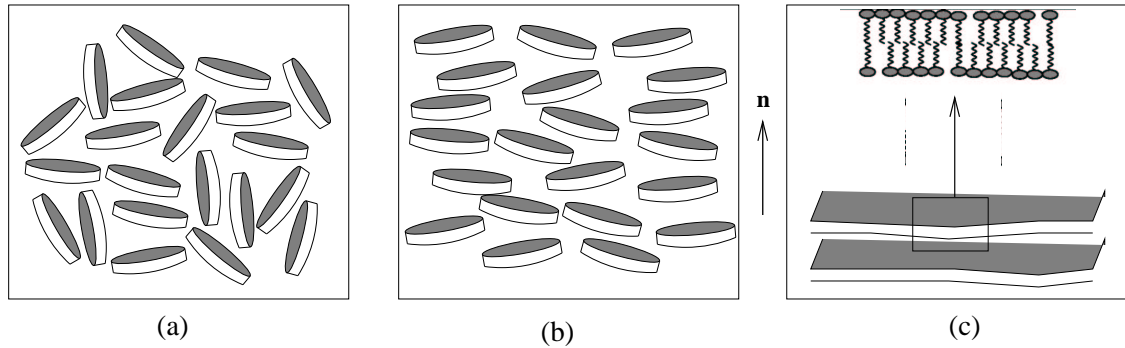
Figure 2.1: A schematic diagram of various phases of CSPFO water system. (a) shows the isotropic micellar phase, (b) is discotic nematic (N_D) micellar phase and (c) is bilayer lamellar phase. These three phases can also be realized by changing the temperature at a certain concentration.

We have carried out systematic studies of the twist viscoelastic coefficient in the N_D phase of CSPFO-water system in a wide range of temperature and concentration. We find that the twist viscoelastic coefficient of CSPFO-water system increases as the temperature in the nematic phase is increased. The twist viscoelastic coefficient is also a sensitive function of the concentration of CSPFO in water at a given reduced temperature.

2.2 Theory

In usual nematics, the rod-like molecules are oriented, on an average, in one direction denoted by the director $\mathbf{n}$. In discotic nematics, the disks are oriented perpendicular to the director. The scattering of light in the liquid crystal medium is mainly due to the thermal fluctuations in the director. These fluctuations can be described by a pair of collective and non propagating modes. At a point r, the director $\mathbf{n_0}(r)$ can be expressed as [15]

$$\mathbf{n_0}(r) = \mathbf{n} + \delta n_1 \mathbf{e_1} + \delta n_2 \mathbf{e_2} \tag{2.1}$$

Here, $\mathbf{n}$ is the director along z-axis, $\mathbf{e_1}$ and $\mathbf{e_2}$ are the two unit vectors along y- and x-axis respectively and δn_1 and δn_2 are the director fluctuations (Fig. 2.2). $\mathbf{q}$ is the wave vector corresponding to the director fluctuations. In scattering experiments $\mathbf{q} = \mathbf{k_i} - \mathbf{k_f}$ where,
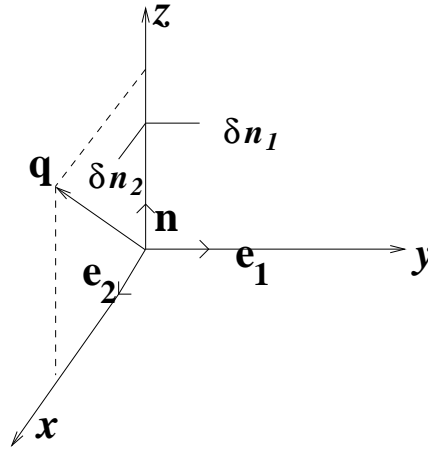
Figure 2.2: The nematic director fluctuations in mode 1 and mode 2 . δn_1 and δn_2 are the components of director fluctuations in the orthogonal yz and zx plane, respectively.

$\mathbf{k_i}$ and $\mathbf{k_f}$ are the wave vectors of incident and scattered light, respectively. The relaxation frequencies corresponding to these modes are given by [15] (see Eqn. (1.29) & (1.30)):

$$\Gamma_i(\mathbf{q}) = \frac{1}{\eta_i(\mathbf{q})} \left(K_{ii}q_\perp^2 + K_{33}q_\parallel^2 \right) \tag{2.2}$$

where $i = 1, 2$ denotes the two modes of fluctuations parallel and perpendicular to the $(\mathbf{n}, \mathbf{q})$ plane. Mode 1 can be probed in H-H scattering geometry while to probe mode 2 one has

to use either V-H or H-V geometry. Here K_{11}, K_{22}, and K_{33} are the Frank elastic constants corresponding to splay, twist, and bend deformation, respectively. η_1 and η_2 are the effective viscosities for mode 1 and mode 2, respectively while $q_{\parallel}$ and $q_{\perp}$ are the parallel and perpendicular components of the wave vector ($\mathbf{q}$) with respect to the director ($\mathbf{n}$). From Eqn. (2.2) it is clear that for $q_{\parallel} = 0$, the measured relaxation frequencies correspond to pure twist deformations for depolarized scattering (V-H geometry). For mode 2 and $q_{\parallel} = 0$ the Eqn. (2.2) becomes:

$$\Gamma = (K_{22}/\eta)q_{\perp}^2 \tag{2.3}$$

where, K_{22}/η is the twist viscoelastic coefficient. Hereafter, we drop the subscript 2 in η_2 and Γ_2. The director fluctuations couple to the incident light via the dielectric tensor. Fluctuations in dielectric tensor give rise to the scattering of light. The intensity auto correlation function of this scattered light is related to field auto correlation function by the Siegert's relation [16] as given by Eqn. (1.15).

$$g_2(\tau, \mathbf{q}) = 1 + \beta|g_1(\tau, \mathbf{q})|^2$$

Here, $g_2(\tau, \mathbf{q})$ and $g_1(\tau, \mathbf{q})$ are the intensity and field correlation functions, respectively and τ is the delay time. The parameter β is coherence factor which depends on the coherence area. In the experimental arrangement, β is a measure of signal to noise ratio.

2.3 Experimental

2.3.1 Instrumentation

The main components of DLS setup are shown in Fig. 2.3. The digital auto correlator was obtained from Malvern Instruments Ltd., U.K. The characteristics of each of the components in the context of DLS experiments are discussed in the following subsections.

2.3.1.1 The light source

Lasers have properties that make them an ideal source for DLS experiments. Our experiments were performed using a 25mw Ar^+ ion laser (Spectra Physics Inc.) with wavelength
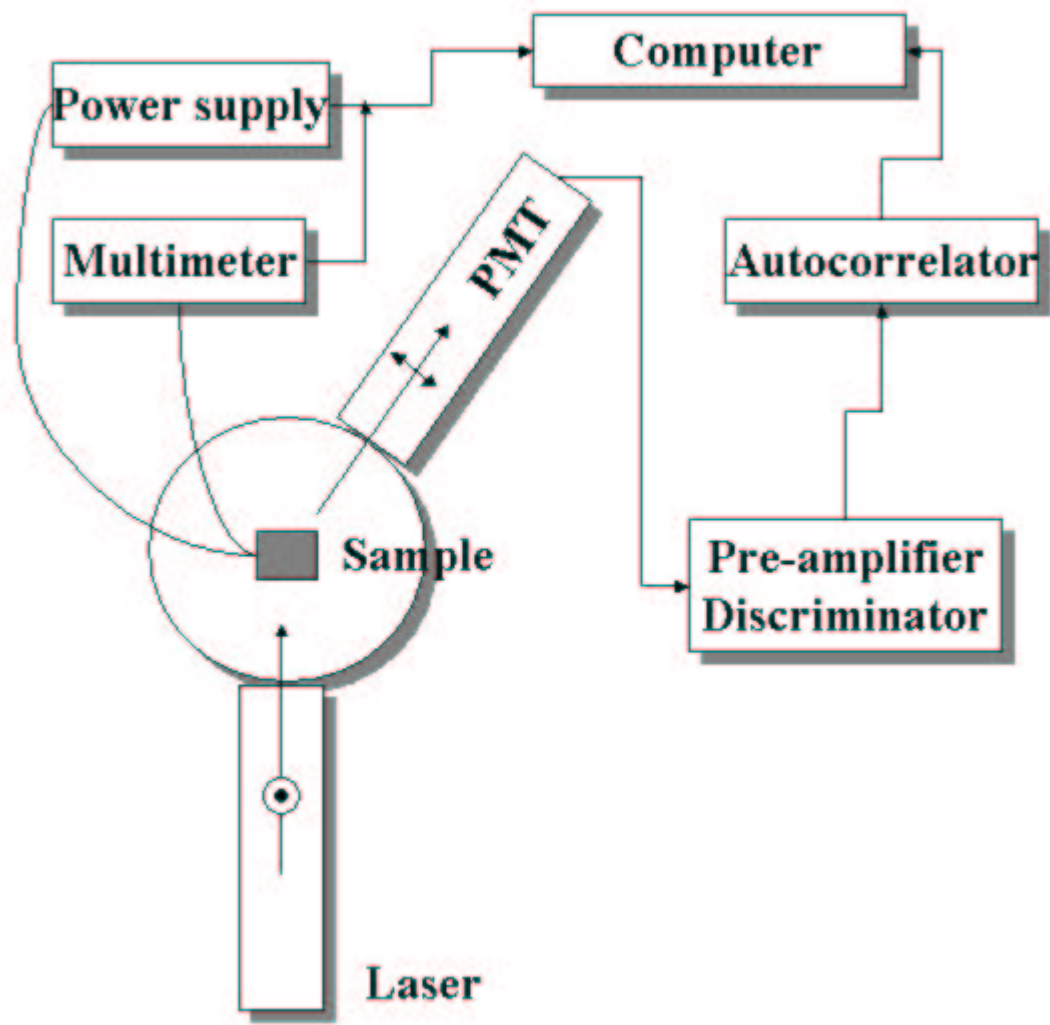
Figure 2.3: The experimental setup for DLS studies.

$488nm$. The output of the laser was linearly polarized. In light scattering experiments from liquid crystals, the scattering arrangement selects particular modes of director fluctuations. This in turn depends on the direction of polarization of the incident and scattered light with respect to the scattering plane.

2.3.1.2   The digital auto correlator

In our experiments, a commercial photon correlator Malvern 4700C was used. Block diagram of an auto correlator is shown in Fig. 2.4. This instrument can operate in two modes, *viz.*, auto correlation and cross-correlation. We have mainly used the correlator to perform auto correlation of a rate modulated pulse train. The digital auto correlator calculates the discrete time autoi correlation of any variable $v(t)$ with a delay time $x\tau$

$$g_2(x\tau) = \sum_{t=1}^{k} v(t)v(t + x\tau) \tag{2.4}$$

where $x = 0, 1, 2....$ and τ is the delay time.

The rate modulated pulse train is a representation of the intensity fluctuations sensed by the detector. These pulses randomly arrive at the correlator input stage, where they are synchronized to a fast basic clock to enable the digital electronics sufficient time to process the pulse. The basic clock defines the resolution of the correlator and normally runs at 10MHz. At the start of each sample a serial to 8-bit parallel conversion process is initiated which results in the number of counts that have arrived in the sample to be represented as an 8 bit number. This 8 bit value is passed down a shift register. The earlier readings advance along the delay register as new ones enter. The multiplication of the current signal and the delayed version is implemented by successive additions. The incoming pulse train is passed down the immediate path to each add/latch (A/L). For every pulse that arrives at the correlator input, the content of each delay register element is added to the sum of the corresponding accumulator. The partial sum accumulated per interval is equal to the number of input pulses multiplied by the 8-bit representation held in a particular element.

Random pulse train

Delay registers

v(t)

Serial to parallel
8–bit conversion

$v(t+\tau)$ $v(t+2\tau)$ $v(t+p\tau)$

A/L   A/L   A/L

Accumulator   Accumulator   Accumulator
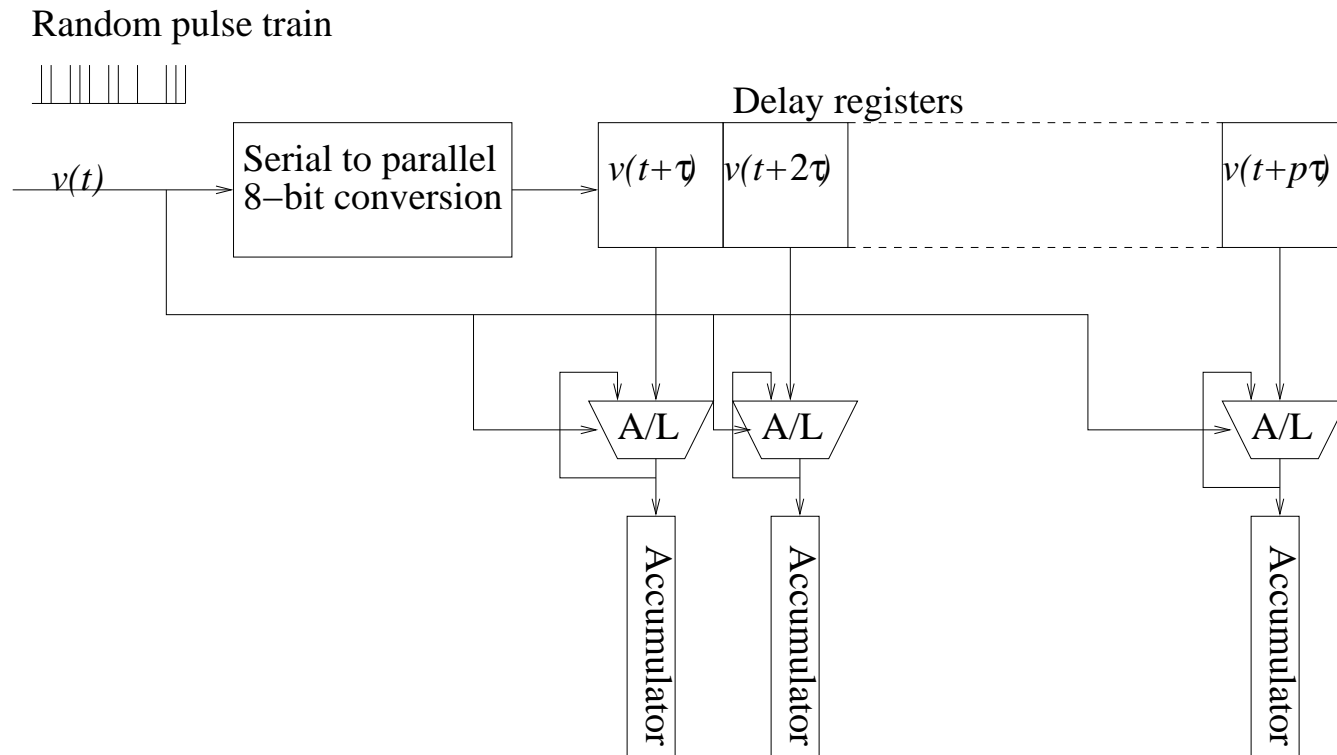
Figure 2.4: The block diagram of digital auto correlator from Malvern Inc. Here, $v(t)$ is the input signal, τ is the delay time, p is the number of channels and A/L represents the add/latch.

2.3.1.3 The light detector

A photomultiplier tube (PMT) obtained from Electron Tubes Ltd. (9863/100KB02) was used as a light detector. It was mounted on a goniometer arm to facilitate us in selecting a wide range of scattering angles. When PMT is operated in photon counting mode, its output is a rate modulated pulse train representing the fluctuating light intensity. A variable size pin hole was kept before PMT and an analyzer was used to select the polarization of scattered light. After electronic processing these signals were fed to the digital auto correlator.

2.3.1.4 The pre-amplifier and discriminator

The signals appearing at the output of PMT are weak as well as contaminated with noise like dark current and secondary pulses. Before feeding these pulses to correlator they need to be processed. These pulses are passed through an electronic module called an amplifier discriminator. This module is used to amplify the signal, suppress the noise and standardize the pulses. Such signals then become suitable for analysis by a digital auto correlator.

2.3.1.5 The sample oven

The dynamics in the scattering medium is sensitive to its temperature. In any systematic investigation, the temperature is an important parameter and hence must be held constant throughout the experiment. The sample oven was fabricated in our workshop. It consists of two blocks of copper firmly joined together. The heating element (Kapton heater from Minco Inc.) was sandwiched between them. Each of the two blocks had a central cylindrical hole to pass the incident laser beam. On the outer side of one block a groove was made to accommodate a capillary tube used as a sample cell. The dimension of the groove was almost same as that of the sample cell for it to exactly fit into the groove. The annular heating elements were used to ensure the uniform heating of the sample. The heater was glued to the copper block with a heat conducting glue in order to ensure good contact between the heater and the copper block. A resistance temperature detector (RTD) was placed in the copper block near the sample, for sensing the temperature. The entire oven was enclosed in a $3mm$

thick Teflon jacket to reduce the heat loss. We have used a PID temperature controller to control the temperature of the sample oven. The algorithm and features of PID controller are described in the next subsection.

2.3.2 PID temperature controller

A controller, compares the measured value from a system with a reference setpoint value. A very effective means of achieving control is to use the Proportional Integral Derivative (PID) algorithm [17]. Unlike simpler control algorithms, the PID controller can adjust the process outputs based on the history and rate of change of the error signal. This gives a more accurate and stable control. Here, we describe briefly the design and fabrication aspects behind the PID temperature controller used for controlling the sample temperature in light scattering experiments. A detailed discussion of the use of PID algorithm for temperature control can be found in literature [18]. In PID algorithm, the voltage applied to the heater coil is a summation of three terms. The first, second and third terms are proportional to the error in temperature, the time integration of the error in temperature and the time derivative of the error in temperature, respectively. The function of the integral control is to reduce the steady state error. The derivative control provides an anticipatory action to reduce the overshoots in the response of the sample oven.

2.3.2.1 Features of control program

The PID temperature control algorithm was implemented in LABView version 6*i*. A digital multimeter (Keithly 2001) was used to perform a 4-probe RTD measurement to sense the oven temperature and a programmable power supply (Aplab 9712P) was used to supply power to the heater. A 10 point moving average was performed on-line over the resistance reading in the program. The PID controller was interfaced to a PC using a standard GPIB card. The oven had a large thermal capacity and hence slow response giving better thermal stability. This allows us to sample the temperature every second. The temperature stability was better than $5mK$. The temperature measurements were monitored on-line. A typical

37

heating and step response curve obtained for the PID temperature controller is shown in Fig. 2.5. The stability of the heater is shown in Fig. 2.6. The PID temperature controller interfaced to a PC and sample oven fabricated in our workshop was used for the experiments described in the present and following chapters.
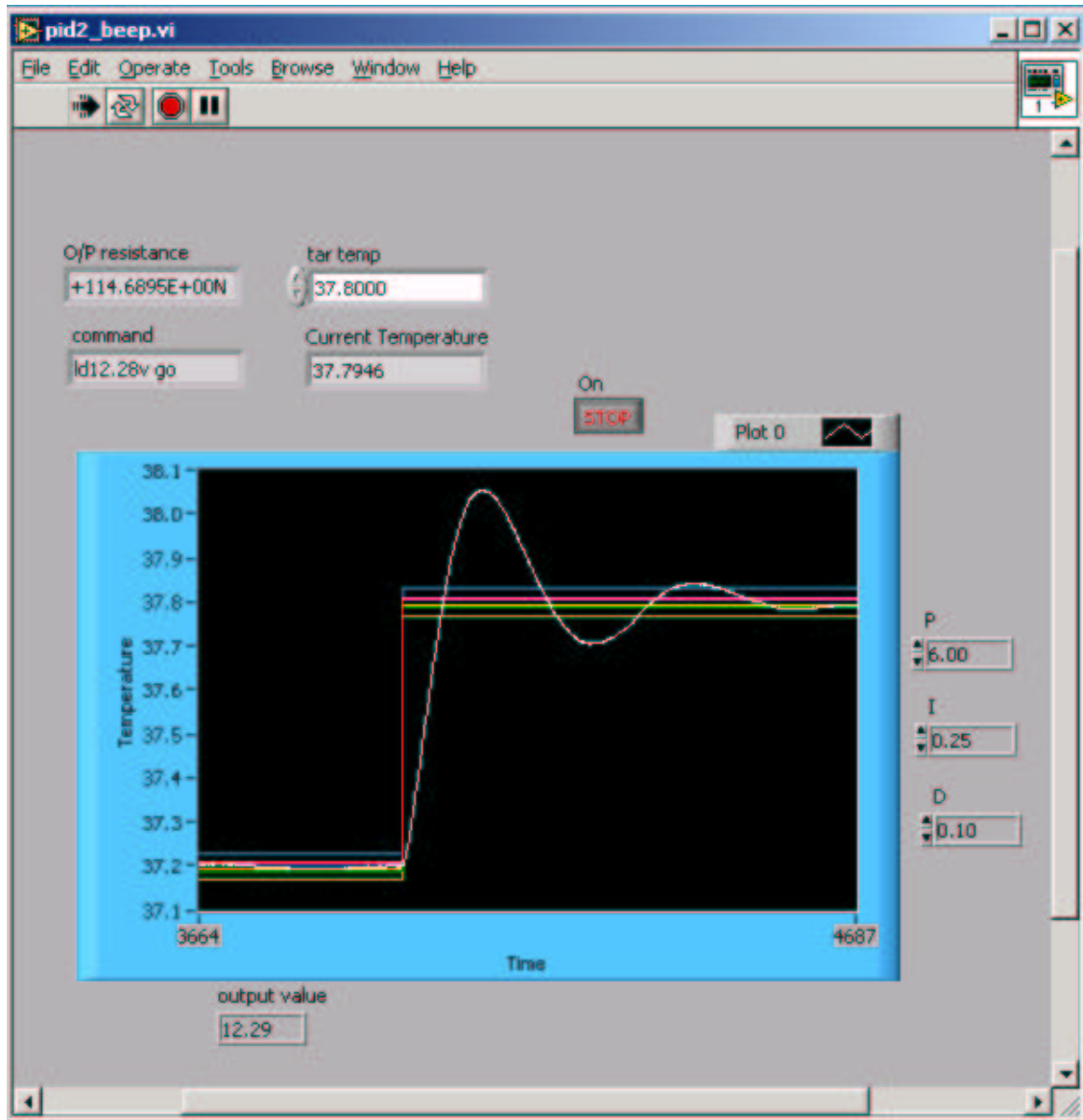
Figure 2.5: The typical step response of a PID temperature controller. Three pairs of parallel lines are plotted to check the accuracy of PID program. The lines in the outer pair represent an accuracy of $\pm 0.03^{o}C$ and the lines in the inner pair represent an accuracy of $\pm 0.005^{o}C$.
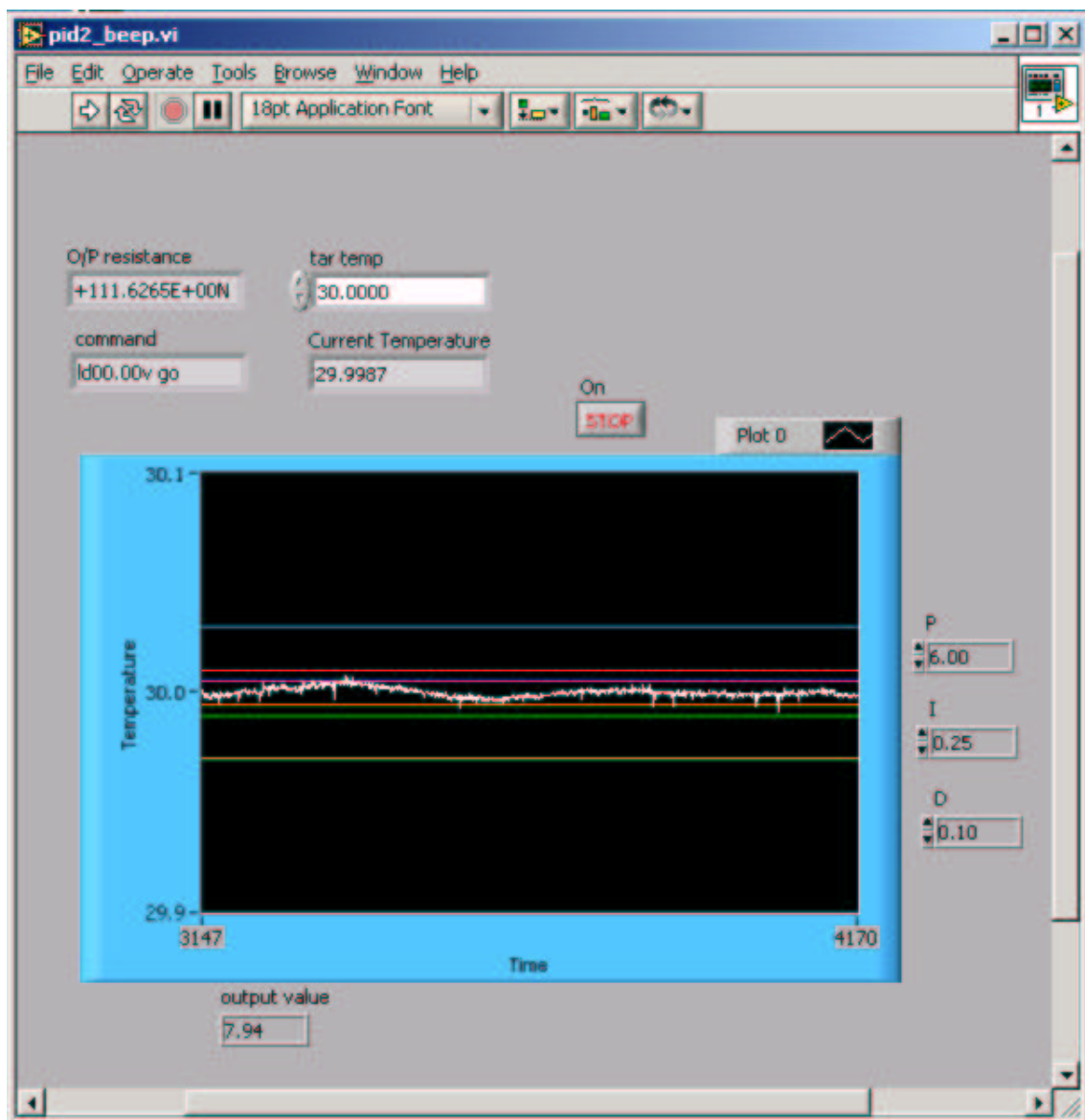
Figure 2.6: The typically obtained temperature stability of PID program at 30.0^oC is better than $5mK$ as shown.

2.3.3 Standard samples

To check the working of the whole setup, we have performed experiments on a few standard samples. Spherical beads of polystyrene with 300 *nm* diameter were purchased from Aldrich. A colloidal solution of these particles was prepared in ultra pure water. It was then filled in a cylindrical tube of diameter 1*cm*. Laser light was incident on this sample and auto correlation was recorded for 60 seconds. We used a special software DYNALS (Alango Ltd.) to analyze the data. The distribution analysis for a standard sample of polystyrene beads, is shown in Fig. 2.7. From the histogram we find that the mean particle radius to be around 150*nm*. The same data was also analyzed by discrete component method and cumulant method. The results obtained were almost same from all the three different analyses. We also performed the experiment at 5 different angles and found the results to be in agreement.
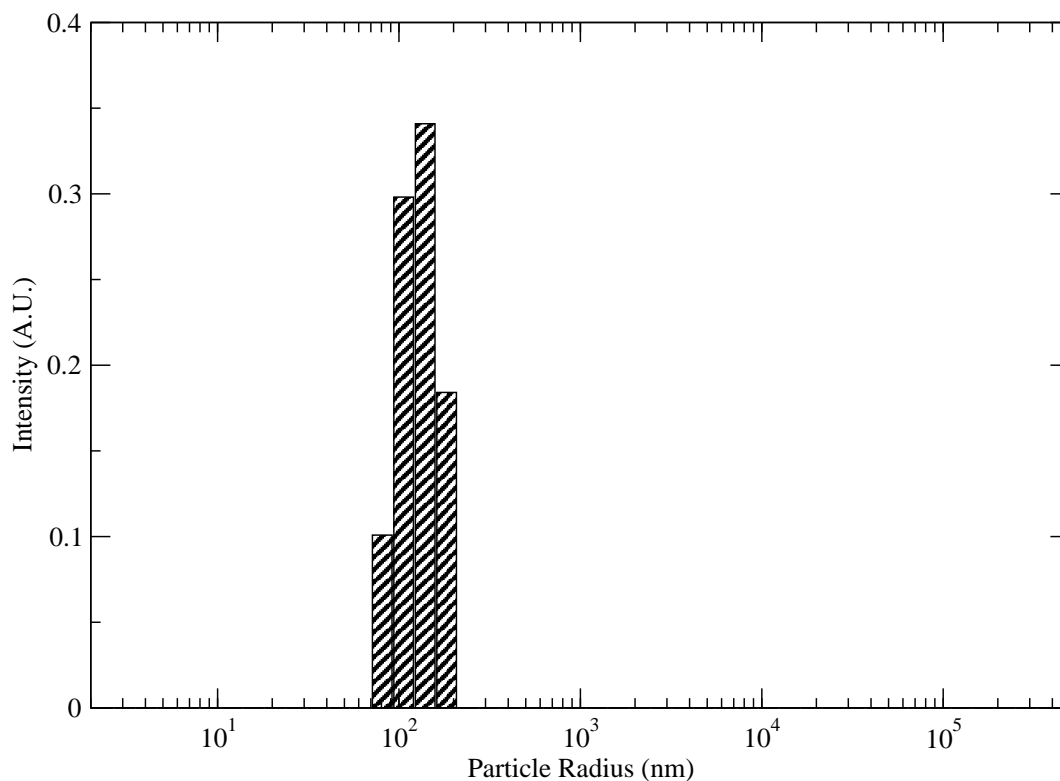
Figure 2.7: The distribution analysis for a standard sample of polystyrene beads of diameter 300*nm* suspended in ultra pure water. The data were taken at a scattering angle of 30° at room temperature. Viscosity of water was taken as 0.89*cP* and refractive index as 1.33.

2.3.4 Sample preparation

The material CSPFO used in the experiment was prepared in our laboratory. We purchased perfluorooctanoic acid and CsOH from Aldrich and used without further purification. Acid was dissolved in pure water and then titrated with an aqueous solution of CsOH to obtain a pH of 7.0. A rotatory evaporator was used to evaporate the extra water. CSPFO was crystallized from ethanol. The crystals so obtained were white and glossy. Ion free ultra pure water obtained from Millipore MilliQ system was used to dissolve CSPFO. After adding CSPFO to water, the solution was kept on a magnetic stirrer for about a day to prepare a homogeneous solution. A flat glass capillary tube (Vitrotubes) of $200\mu m$ thickness was used as a sample cell. The sample cell was then flame sealed at both ends to avoid evaporation of water from the mixture. The sample cell was kept vertically in the sample holder. The sample temperature was controlled by using a PID algorithm as described in the previous subsection. Transition temperature of the sample was checked with the help of a polarizing microscope before and after the experiment. A typical Schlieren texture of the unaligned nematic phase of CSPFO water system is shown in Fig. 2.8. The sample was aligned homeotropically (with the director perpendicular to the flat glass surface) by slow cooling from the isotropic phase and then keeping it just below the transition temperature for about an hour. Before doing the experiment, the alignment was checked by conoscopy. A typical conoscopic image of the aligned nematic is shown in Fig. 2.9

In the DLS experiments, laser beam propagated along the director and it was polarized perpendicular to the scattering plane. Scattered light was detected using PMT mounted on a goniometer arm. A $200\mu m$ pin hole was selected in between the analyzer and the PMT to collect the scattered light over a small coherence area. The photo current generated by PMT was processed as described in the previous section and was then fed to the digital correlator. This digital correlator facilitated in computing the intensity auto correlation of scattered light.

Figure 2.8: A polarizing microscope image of CSPFO water system in the nematic (N_D) phase showing a schlieren texture. The magnification was 200× and sample was kept between crossed polarizers.
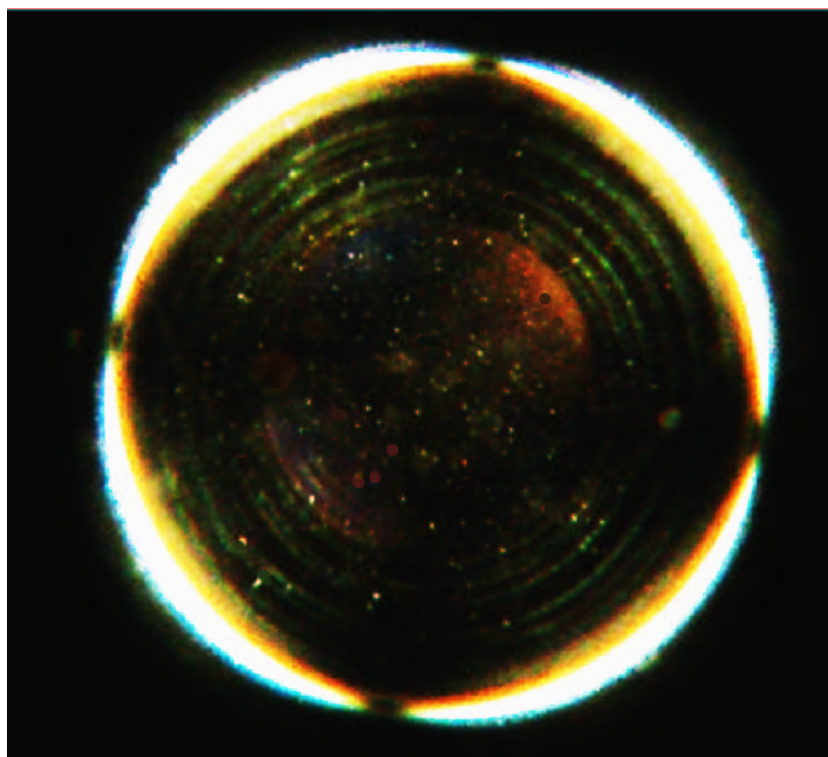
Figure 2.9: A conoscopic texture of homeotropically aligned nematic phase of CSPFO water system seen under a polarizing microscope.

2.3.5 Experimental geometry

The experiment was carried out in the homodyne regime, where, the Siegert's relation holds good [4]. We have chosen the scattering angles to be small enough such that scattering wave vector ($\mathbf{q} = \mathbf{k_i} - \mathbf{k_f}$) is nearly perpendicular to the director (shown in Fig. 2.10). The
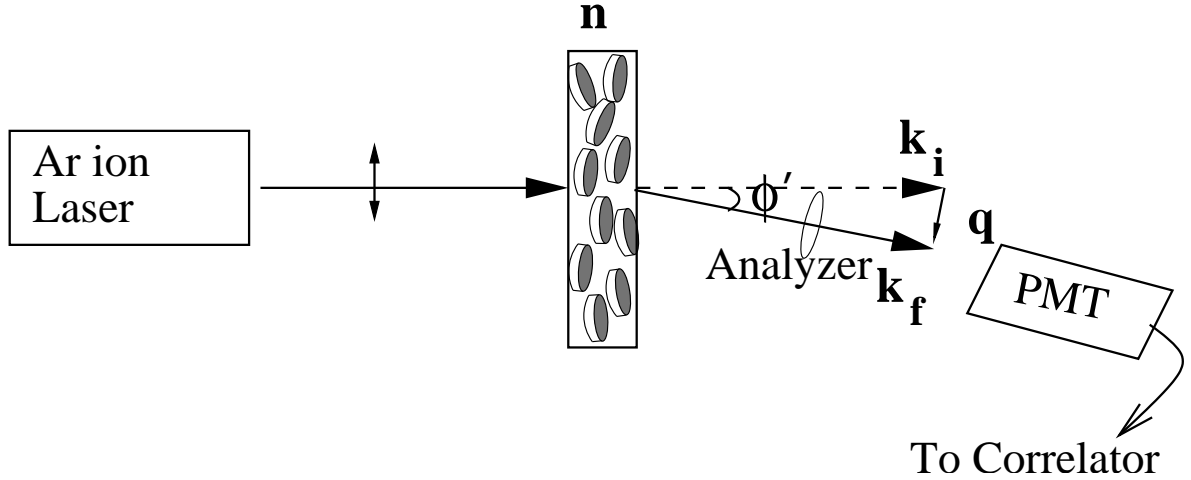
Figure 2.10: The experimental geometry for observing twist viscoelastic coefficient.

magnitude of the scattering wave vector ($\mathbf{q}$) is given by the following relation:

$$|\mathbf{q}| = \frac{4\pi\bar{n}}{\lambda} sin\left(\frac{\phi}{2}\right) \tag{2.5}$$

Here, $\bar{n}$ is average refractive index of the medium, λ is the wavelength of light and ϕ is the scattering angle. The measured value of the scattering angle (ϕ') was corrected for the refraction at glass-air interface by the following equation:

$$\phi = sin^{-1}\left[\frac{1}{\bar{n}} sin\phi'\right] \tag{2.6}$$

The value of average refractive index of the liquid crystalline medium does not change much as a function of temperature. Hence, we have neglected the temperature variation of $\mathbf{q}$. In our experiment, for all angles, we have calculated the value of $(q_{\parallel}/q_{\perp})^2$ which was always found to be less than 0.03. Also, it is known that the ratio between K_{22} and K_{33} for thermotropic discotic molecules [19] is approximately 5. We assume a similar behavior for lyotropic discotic systems and hence, the quantity $K_{33}q_{\parallel}^2$ can be neglected with respect to $K_{22}q_{\perp}^2$ in

43

Eqn. (2.2). Thus, in this geometry, the relaxation frequency corresponds to pure twist mode as given in Eqn. (2.3).

2.4 Results

We have analyzed our data by fitting the correlation function to a single exponential decay given by the following expression

$$g_2(\tau, \mathbf{q}) = A + B e^{-2\Gamma\tau} \tag{2.7}$$

where, A and B are constants, Γ is the relaxation frequency and τ is the delay time. For detecting the twist mode (*i.e.* mode 2) we have chosen incident polarization to be perpendicular to the scattering plane (V), while the scattered light was analyzed in a direction parallel to the scattering plane (H). In Fig. 2.11, a typical auto correlation function obtained in our experiment is shown. The solid line represents a single exponential fit to the experimental data. The value of twist relaxation frequency (Γ) was deduced from the fit. Since the auto correlation function fits quite well to a single exponential decay, it follows that in the geometry depicted in Fig. 2.10, the contribution due to bend fluctuations is negligible. We have measured the values of relaxation frequencies (Γ) corresponding to the V-H configuration at nine different scattering angles. The relaxation frequencies as a function of q^2 for the concentration of 50% CSPFO in water, at five different temperatures are shown in Fig. 2.12. We find that our data fit well to the straight lines passing through the origin. The corresponding slopes give the twist viscoelastic coefficient as a function of temperature for a given concentration of CSPFO.

We have performed the experiment for five different concentrations of CSPFO in water. In Fig. 2.13, the twist viscoelastic coefficient is depicted as a function of reduced temperature $(T - T_{NI})$ for various concentrations.
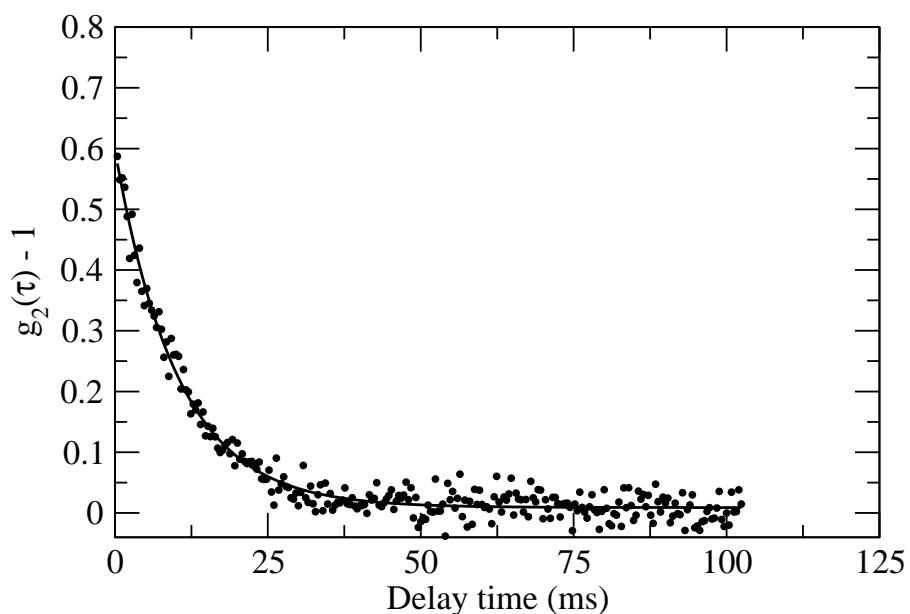
Figure 2.11: A typical auto correlation function obtained from our experiments for 45% (w/w) of CSPFO in water at $34.0^o C$. The scattering angle was 17.7^o. Solid line is a fit given by Eqn. (2.7). The value of relaxation frequency deduced from the fit is $48.86 Hz$
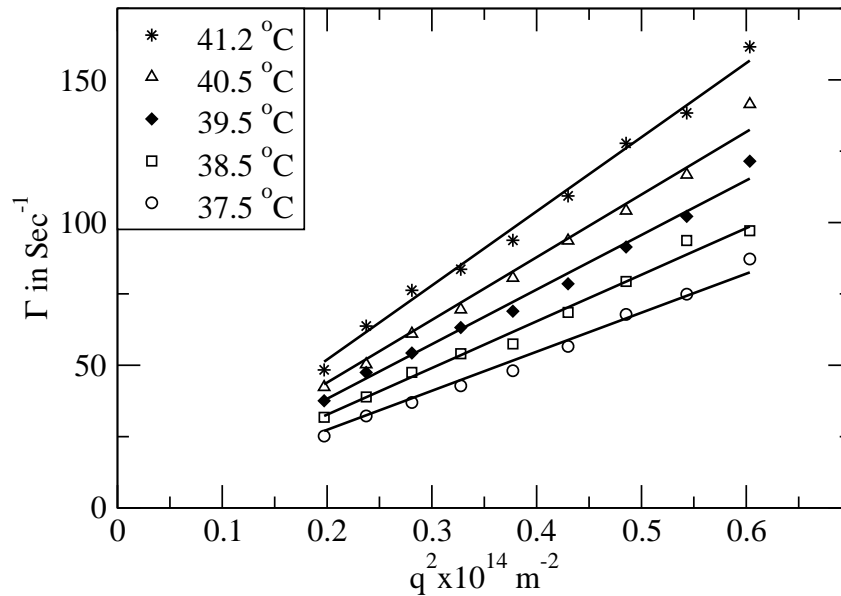
Figure 2.12: The variation of the twist relaxation frequency (Γ) with the square of wave vector at different sample temperatures. The concentration of CSPFO in water was 50% (w/w). The solid lines are fits to the experimental data using Eqn. (2.3).
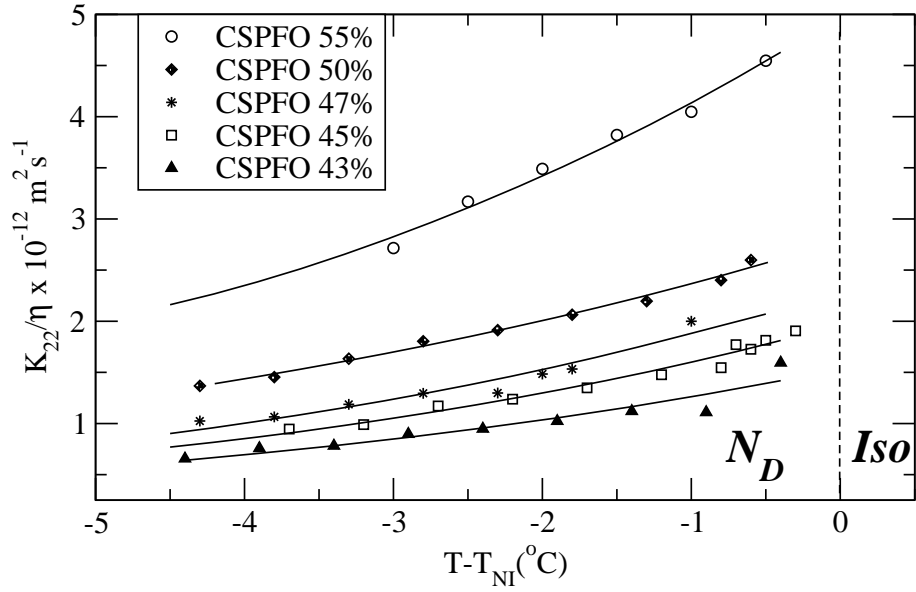
Figure 2.13: The variation of twist viscoelastic coefficient as a function of reduced temperature for various concentrations. Solid lines are a cue to the eyes.

2.5 Discussion

We find that the twist viscoelastic coefficient increases with temperature in the nematic phase as shown in Fig. 2.13. Generally, elastic constants decrease with increase in temperature. Hence, our results implies that the variation of twist viscoelastic coefficient is dominated by the variation of viscosity, in the range of temperature considered here. In Table (2.1) we compare our values of K_{22}/η, with the values reported in literature for other systems [6, 12, 15]. The values of K_{22}/η for 50% CSPFO in water, obtained by us are rather close to the values reported in lyotropic discotic nematic system of Potassium Laurate(KL)/Decanol/water [12]. We find that the values of K_{22}/η for CSPFO water system are of the same order of magnitude as twist viscoelastic coefficient of the thermotropic discotic nematic [6], while in the case of usual thermotropic nematics, the values are much higher [15]. At a given reduced temperature, K_{22}/η increases rapidly with increase in the concentration of CSPFO in water (see Fig. 2.14). At lower concentrations of CSPFO in water K_{22}/η slowly increases, whereas at higher concentrations it rapidly rises with the concentration. This shows that surprisingly the twist viscosity decreases with increasing concentration of CSPFO in water. We would like

to point out here that a systematic study of viscoelastic coefficient of lyotropic nematic as a function of temperature and concentration has not been reported in literature. In this chapter we have described a systematic study for CSPFO water system.

Table 2.1: Twist viscoelastic coefficient for CSPFO-water system compared with typical values for some other systems.

Sample	Phase	Temperature	$K_{22}/\eta(m^2 s^{-1})$	Ref.
CSPFO/water 50/50 by Wt.	Lyotropic (N_D)	39.5^oC	1.9×10^{-12}	[20]
(HATX)$C_{12}H_{25}$	Thermotropic (N_D)	65^oC	0.42×10^{-12}	[6]
$KL/Decanol/D_2O$ 25.5/6.32/68.53 by Wt.	Lyotropic (N_D)	19^oC	1.6×10^{-12}	[12]
MBBA	Thermotropic (N)	25^oC	4.3×10^{-11}	[15]
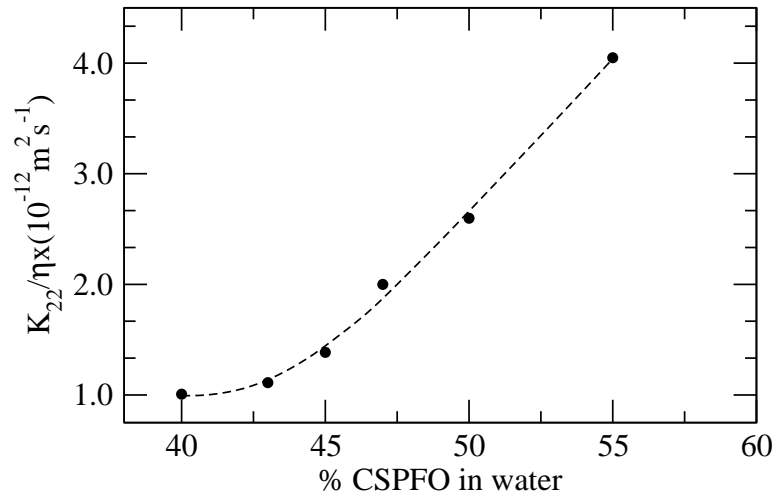
Figure 2.14: Twist viscoelastic coefficient variation with the concentration of CSPFO in water. The data are plotted at the reduced temperature $(T_{NI} - T)$ of 1.0^oC. The dashed line is a cue to the eyes.

2.5.1 Estimation of the activation energy

The flow activation energy is the minimum energy required to induce flow in a system at rest. From the experimental data, we have estimated the activation energy corresponding to twist

viscosity in the director. We have taken the usual temperature dependence of viscosity (η) and twist elasticity (K_{22}), and we have used our results of K_{22}/η as a function of temperature to estimate the activation energy (E_a). There are many reports on the temperature dependence of twist viscosity (η) of liquid crystals. According to the molecular model of Diogo and Martins, η varies as order parameter (S) squared [21], while the data for real liquid crystals fit the following equation [15, 22, 23]:

$$\eta(T_A) \propto S(T_A)e^{E_a/k_B T_A} \tag{2.8}$$

where S is the order parameter, E_a is the activation energy, k_B is the Boltzmann's constant and T_A is the absolute temperature. The temperature dependence of K_{22} can be taken as [15]:

$$K_{22}(T_A) \propto S^2(T_A) \tag{2.9}$$

The values of order parameter (S) were obtained from literature [24]. The data of $ln(K_{22}/\eta S)$ with temperature was fitted using the following Eqn.:

$$ln\left(\frac{K_{22}}{\eta S}\right) = A_0 - E_a/k_B T_A \tag{2.10}$$

The result is depicted in Fig. 2.15. The fitting parameter gives us the value of activation energy. The value of E_a from our data is found to be around 60.4 ± 2.4 Kcal/mole for 50% CSPFO in water (see Fig. 2.15). In Table (2.2) the values of activation energy (E_a) of CSPFO-water system is compared with the other liquid crystalline systems. For the lyotropic system of CTAB and water it is found to be of the order of $27 Kcal/mole$ [25]. For usual thermotropic nematic systems, E_a is rather low [23]. For lyotropic cholesteric liquid crystals, it depends on the amount of chiral dopant in lyotropic nematic [26]. For thermotropic cholesteric it is less than that for cholesteric lyotropic [10]. Polymeric liquid crystals have relatively higher activation energy [27].

For the N_D phase of CSPFO-water system, the order parameter is not a very sensitive function of concentration of CSPFO in water [24]. Hence, we fit our data on K_{22}/η at other concentrations of CSPFO using S values reported by Jolley *et.al.* [24]. We find that the activation energy is independent of the concentration of CSPFO in water.
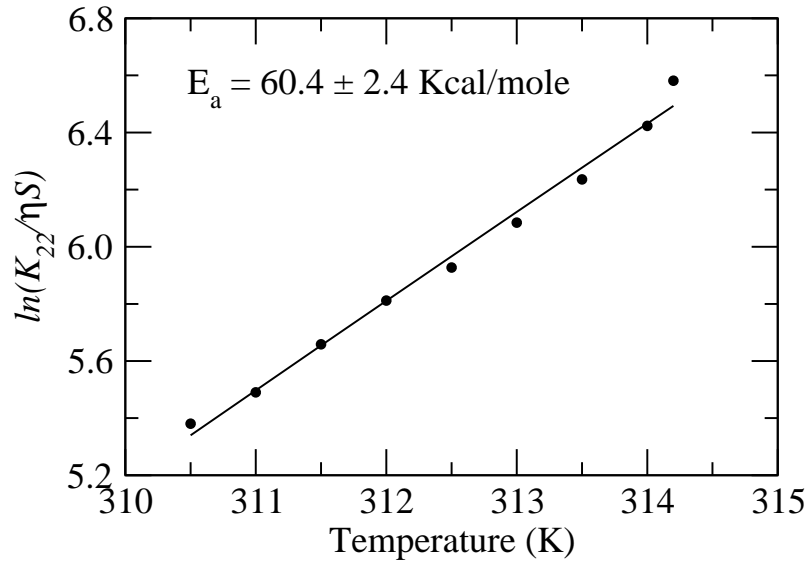
Figure 2.15: The variation of $ln(K_{22}/\eta S)$ as a function of temperature. The solid line is a fit given by Eqn. (2.10) to our data for 50% CSPFO in water.

Table 2.2: Activation energy for CSPFO water system compared with other liquid crystal systems.

Sample	E_a (*Kcal/mole*)	**References**
CSPFO/water	≈ 60	[20]
CTAB/water/KBr	≈ 27	[25]
Nematic (MBBA)	≈ 12	[23]
Cholesteric (lyotropic)	$\approx 65 - 80$	[26]
Cholesteric (thermotropic)	≈ 27	[10]
Polymer liquid crystal	≈ 95	[27]

In this chapter, we have studied the twist viscoelastic coefficient of lyotropic discotic nematic liquid crystals. We also estimate the activation energy corresponding to twist, from our data and find that activation energy is not a sensitive function of concentration of surfactant in water. The addition of some complex molecules in lyotropic systems is important from biological point of view. In the next chapter we describe our studies on the dynamic light scattering from lyotropic discotic nematic liquid crystal doped with various molecules.

Bibliography

[1] Gelbart W.M., Ben-Shaul A. and Roux D., *Micelles, membranes, micro-emulsions, and monolayers*, Springer Verlag, New York 1994.

[2] Holmes M.C., Reynolds D.J. and Boden N., *J. Phys. Chem.*, **91** pp. 5257 (1987).

[3] Boden N., Corne A.S. and Jolley K.W., *J. Phys. Chem.*, **91** pp. 4092 (1987).

[4] Berne B.J. and Pecora R. *Dynamic Light Scattering*, Wiley-Interscience publication, Toranto, 1976.

[5] Hasegawa M., Miyachi K. and Fukuda A., *Japan J. Appl. Phys.*, **34** pp. 5694 (1995).

[6] Othman T., Gharbia M., Gharbi A., Destrade C. and Durand G., *Liq. Cryst.*, **18** pp. 839 (1995).

[7] Sah Y. and Suresh K.A., *Liq. Cryst.*, **24** pp. 701 (1998).

[8] Derbel N., Othman T. and Gharbi A., *Liq. Cryst.*, **25** pp. 561 (1998).

[9] Kubono A., Yoshino K., Ninomiya T., Akiyama R. and Tanaka K., *Liq. Cryst.*, **29** pp. 1089 (2002).

[10] Giridhar M.S. and Suresh K.A., *Euro. Phys. J. E*, **7** pp. 167 (2002).

[11] Duke, R.W. and Du Pre D.B., *Phys. Rev. Lett.*, **33** pp. 67 (1974).

[12] Lacerda-Santos M.B., Galerne Y. and Durand G., *J. de Phys.*, **46** pp. 933 (1985).

[13] Lacerda-Santos M.B. and Amato M., *Euro. Phys. J. B*, **7** pp. 393 (1999).

[14] Yamamoto J. and Tanaka H., *Nature*, **409** pp. 321 (2001).

[15] De Gennes P.G. and Prost J., *The Physics of Liquid Crystals*, Oxford University Press, UK, 2001.

[16] Lemieux P.A. and Durian D.J., *J. Opt. Soc. Am. A*, **16** pp. 1651 (1999).

[17] Franklin G.F., Powell J.D. and Workman M., *Digital control of dynamic systems*, Addison-Wesley, 2000.

[18] Benjamin C.K., *Digital control systems*, Holt, Rinehart and Winston Inc. 1980.

[19] Sokalaski K. and Ruijgrok Th.W., *Physica A*, **113** pp. 126 (1982).

[20] Agarwal A.K. and Suresh K.A., *Proc. of SPIE*, **5947** pp. 59470A (2005).

[21] Diogo A.C. and Martins A.F., *Mol. Cryst. Liq. Cryst.*, **66** pp. 133 (1981).

[22] Prost J., Sigaud G. and Regaya B., *J. de. Phys. Lett.*, **37** pp. L341 (1976).

[23] de Jeu W. H., *Phys. Lett. A*, **69A** pp. 122 (1978).

[24] Jolley K.W., Boden N., Parker D. and Henderson J.R., *Phys. Rev. E*, **65** pp. 41713 (2002).

[25] Candau S.J., Hirsch E., Zana R. and Delsanti M., *Langmuir*, **5** pp. 1225 (1989).

[26] Alacantra M.R., de Moura A.F. and Fernandes E.G. Jr., *Liq. Cryst.*, **29** pp. 191 (2002).

[27] Tormes M., Munoz M.E., Pena J.J. and Santamaria A., *J. Poly. Sci.: Part B: Poly. Phys.*, **36** pp. 253 (1998).